Food Chemistry 309 (2020) 125743

Contents lists available at ScienceDirect

Food Chemistry

journal homepage: www.elsevier.com/locate/foodchem

# Study on the molecular interactions of hydroxylated polycyclic aromatic hydrocarbons with catalase using multi-spectral methods combined with molecular docking

Jing Zhang[a], Linfeng Chen[b], Yaxian Zhu[c], Yong Zhang[b,*]

[a] Key Laboratory of Estuarine Ecological Security and Environmental Health, Tan Kah Kee College, Xiamen University, Zhangzhou 363105, PR China
[b] State Key Laboratory of Marine Environmental Sciences of China, College of Environment and Ecology, Xiamen University, Xiamen 361102, PR China
[c] Department of Chemistry, College of Chemistry and Chemical Engineering, Xiamen University, Xiamen 361005, PR China

ARTICLE INFO

*Chemical compounds studied in this article:*
1-hydroxynaphthalene (PubChem CID: 7005)
9-hydroxyphenanthrene (PubChem CID: 10229)
1-hydroxypyrene (PubChem CID: 21387)

*Keywords:*
Hydroxylated polycyclic aromatic hydrocarbons
Catalase
Binding interaction
Spectroscopic techniques
Molecular docking

ABSTRACT

To reveal the potential effects of hydroxylated polycyclic aromatic hydrocarbons (OH-PAHs) on catalase (CAT), the interactions of 1-hydroxynaphthalene (1-OHNap), 9-hydroxyphenanthrene (9-OHPhe) and 1-hydroxypyrene (1-OHPyr) with CAT were investigated using multi-spectroscopic and molecular docking techniques. Fluorescence analysis showed that 1-OHNap, 9-OHPhe and 1-OHPyr can form 1:1 complex with CAT, with the binding constant of $6.31 \times 10^3$, $1.03 \times 10^4$ and $2.96 \times 10^5$ L mol$^{-1}$ at 17 °C. Thermodynamic and docking parameters demonstrated that van der Waals' force, hydrogen bonds and hydrophobic interactions dominated the three binding processes. Molecular docking also revealed the specific binding mode of OH-PAHs with CAT. Synchronous fluorescence and circular dichroism spectral results indicated that the three OH-PAHs induced varied structural changes of CAT. Furthermore, CAT activity was promoted by 9-OHPhe, but inhibited by either 1-OHNap or 1-OHPyr. Under the maximum experimental concentration of OH-PAHs, the percent change of CAT activity induced by 1-OHNap, 9-OHPhe and 1-OHPyr were 8.42%, 4.26% and 13.21%.

## 1. Introduction

Polycyclic aromatic hydrocarbons (PAHs), as typical persistent organic pollutants, can accumulate in human beings through food intake, as they may be formed during the process of food preparation, such as barbecuing, smoking, or frying (Gysel et al., 2018; Lao et al., 2018). After entering the human body, parent PAHs can be primarily metabolized by cytochrome P450 enzymes and converted to more active oxy-derivatives such as epoxides and hydroxyl compounds. These metabolites have the potential ability to bind with biomacromolecules (e.g., DNA and proteins), which may induce damage to the DNA or the proteins (Moorthy, Chu, & Carlin, 2015). Therefore, the investigations on the molecular interactions between biomacromolecules and the oxygenated metabolites of PAHs are of importance to understand the toxic effects of PAHs. Hydroxylated polycyclic aromatic hydrocarbons (OH-PAHs), a type of important metabolites of PAHs, are considered to be potentially more toxic than their parent PAHs (Diamante et al., 2017), while they have not been studied extensively as their parent PAHs. Hence, more attention should be paid to the molecular interactions of OH-PAHs with functional biomacromolecules and the corresponding effects.

Catalase (CAT, EC 1.11.1.6) is a heme containing metalloenzyme, which catalyzes the degradation of hydrogen peroxide ($H_2O_2$) into one molecule of $H_2O$ and a half molecule of $O_2$ (Deisseroth & Dounce, 1970), thus playing an important role in protecting cells from oxidative injure induced by reactive oxygen species (ROS). As is well-known, ROS have been considered to be an important factor in aging, cancer, diabetes, hypertension and inflammation, and thus the denaturation of CAT is correlated with these pathological states (Glorieux & Calderon, 2017). Recently, more and more studies have been performed on the potential toxicity of pollutants on CAT *in vivo* and *in vitro*. Intake of exogenous environmental pollutants is suggested to cause the conformational destruction of CAT and/or to affect the catalytic activity of CAT (Chen, Zhang, Zhu, & Zhang, 2018; Wang, Wang, Xu, Liu, & Chen, 2016; Xu et al., 2018). Even so, the toxicity mechanism of pollutants on CAT is still far from being fully understood.

As the toxicity of contaminants is originated from their interactions with functional biomacromolecules (Moorthy et al., 2015), the

* Corresponding author at: State Key Laboratory of Marine Environmental Science of China (Xiamen University), College of Environment and Ecology, Xiamen University, 361102 Xiamen, Fujian Province, China.
*E-mail addresses:* yaxian@xmu.edu.cn (Y. Zhu), yzhang@xmu.edu.cn (Y. Zhang).

https://doi.org/10.1016/j.foodchem.2019.125743
Received 1 October 2018; Received in revised form 11 September 2019; Accepted 17 October 2019
Available online 21 October 2019

investigation on the molecular interactions of OH-PAHs with CAT are crucial to reveal the toxicity mechanism of OH-PAHs on the antioxidant enzyme system. In our previous work, the interaction between CAT and 1-hydroxypyrene (1-OHPyr) were preliminary investigated (Chen, Zhang, Zhu, & Zhang, 2015), and the strong binding affinity of 1-OHPyr to CAT and the adverse effect of 1-OHPyr on the conformation and function of CAT were confirmed. However, minor changes in the structure of OH-PAHs may induce their different interaction behaviors with biomacromolecules and govern their toxicity in organisms (Sievers, Shanle, Bradfield, & Xu, 2013; Wang, Wang, Chen, & Guo, 2009). Wu et al. (Wu, Wu, Guan, Su, & Cai, 2007) proved the formation of the complex between hydroxynaphthalene and bovine serum albumin (BSA), and revealed that the binding of 1-hydroxynaphthalene (1-OHNap) with BSA was more cooperative than that of 2-hydroxynaphthalene. Wang et al. (2009) investigated the binding of 26 OH-PAHs with DNA, which suggested that steric effect was vital in the interaction of DNA with differently substituted OH-PAH. Ohura, Kurihara, and Hashimoto (2010) investigated the binding interactions between OH-PAHs and aryl hydrocarbon receptor (AhR), and the results indicated that the number and site of hydroxy-groups substituted on PAH skeleton obviously influenced the AhR-ligand binding capacity of OH-PAHs, with the octanol-water partition coefficient ($K_{ow}$) value of OH-PAH significant related to the AhR activity. Li et al. (2011) developed a QSAR model to characterize the interactions of OH-PAHs with DNA, which suggested that the electrostatic potential, molecular size and polarizability of OH-PAHs were closely correlated with their binding capacity to DNA. Sievers et al. (2013) reported that 1-OHNap, 9-hydroxyphenanthrene (9-OHPhe) and 1-hydroxypyrene (1-OHPyr) were able to competitively bind ERβ, induce ERβ homodimers, and regulate ERβ target genes, whereas, the relative activity of each compound is quite different. These studies confirmed that the binding affinity/the adverse effects of OH-PAHs to/on biomacromolecules varied as the structural difference of OH-PAHs. Specifically, the log$K_{ow}$, charges and steric effect of OH-PAHs are important factors affecting the binding interactions. Therefore, in order to fully understand the effects of the structural difference of OH-PAHs on their interactions with CAT, further work on different OH-PAHs with varied number of benzene rings should be conducted.

Herein, based on our previous work, the interactions of CAT with 2–4 ring monohydroxy PAHs (1-OHNap, 9-OHPhe and 1-OHPyr) were further investigated in the present study. Briefly, this work is undertaken based on the following hypothesis: 1) OH-PAHs with different numbers of aromatic rings may have varied binding affinity to CAT, and the binding ability of CAT with OH-PAHs may be associated with the hydrophobicity of OH-PAHs; 2) OH-PAHs with different numbers of aromatic rings can induce different structural and functional changes of CAT, due to the varied molecular interaction of OH-PAHs with CAT. To verify these hypotheses, firstly, multi-spectroscopy, in combination with molecular docking method, was employed to study the binding information of OH-PAHs with CAT. Then, synchronous fluorescence and circular dichroism (CD) spectroscopy methods were employed to clarify the effects of the binding interactions on the structure of CAT. Enzyme activity measurements were further utilized to interpret the response of CAT activity after OH-PAHs exposure. Meanwhile, the differences of the interactions of CAT with OH-PAHs with different numbers of aromatic rings were discussed throughout the study. These investigations aim to help clarify the molecular mechanism of the interactions between CAT and OH-PAHs, and provide an important basis for further understanding the toxicity of OH-PAHs on antioxidant enzyme systems *in vivo* and further warn the health risk of the PAHs *via* dietary intake.

## 2. Materials and methods

### 2.1. Materials

Three OH-PAHs (1-OHNap, 9-OHPhe, and 1-OHPyr) with purity > 99% and CAT from bovine liver were purchased from Sigma-Aldrich Company, USA. 30% $H_2O_2$ was from Xilong Chemical Company, Ltd, China. Stock solutions of $5.0 \times 10^{-5}$ mol $L^{-1}$ CAT were prepared in Tris-HCl buffer. $1.0 \times 10^{-2}$ mol $L^{-1}$ 1-OHNap, $2.0 \times 10^{-3}$ mol $L^{-1}$ 9-OHPhe and $2.0 \times 10^{-3}$ mol $L^{-1}$1-OHPyr were all prepared in ethanol and stored at 4 °C in the dark. All chemicals were of analytical grade, and ultrapure water (> 18.2 MΩ $cm^{-1}$) was used throughout the experiments.

### 2.2. Methods

All of the samples were prepared in a series of 10 mL colorimetric tubes and were diluted with 0.05 mol $L^{-1}$ Tris–HCl buffer (containing 0.10 mol $L^{-1}$ NaCl, pH = 7.40) to volume, and mixed. Exceptionally, the samples used for CD measurements were diluted with ultrapure water. Each sample should contain no more than 5‰ (v/v) ethanol. Besides, the sample balance placing time was 20 min (unless explicitly stated). All measurements were conducted at 17 °C and performed in triplicate (unless explicitly stated).

#### 2.2.1. Fluorescence spectra measurements

The fluorescence quenching experiments were performed at three different temperatures (17, 27 and 35 °C), after maintained the samples in a thermostatic water bath for 1 h. The steady-state fluorescence spectra of the samples were measured on a Cary Eclipse fluorescence spectrophotometer (Varian, USA), with the excitation/emission slit widths of 5/10 nm, respectively. The fluorescence emission spectra were recorded in the range of 290–550 nm at the excitation wavelength of 280 nm. The synchronous fluorescence spectra were scanned at $\Delta\lambda$ = 15 nm (excitation wavelength from 270 to 310 nm), and $\Delta\lambda$ = 60 nm (excitation wavelength from 250 to 310 nm).

#### 2.2.2. CD spectra measurements

CD spectra of the CAT in different systems were measured from 200 to 250 nm in 1.0 nm intervals with a JASCO-810 spectrometer (Shimadzu, Japan), at the scanning speed of 500 nm $min^{-1}$. Each CD spectrum of the CAT was the average of three scans, and was baseline corrected by subtracting the spectrum of the corresponding solutions without CAT. The secondary structural contents of the CAT were calculated by CDpro software combined with the CONTIN/LL method.

#### 2.2.3. Molecular docking process

AutoDock 4.2.6 software and Autodock Tool (ADT) (the Scripps Research Institute, La Jolla, CA, USA) (Morris et al., 2009) were employed to perform the molecular docking processes of the interactions of 1-OHNap, 9-OHPhe, or 1-OHPyr with CAT. GaussView 5.0.8 program (the Gaussian Inc., Pittsburgh, PA, USA) was utilized to draw the three-dimensional (3-D) structures of 1-OHNap, 9-OHPhe and 1-OHPyr. The obtained structures were further optimized by Gaussian 09 software package (Frisch et al., 2009) using the DFT/B3LYP method combined with the 6-31G(d) basis set. The native structure of CAT was obtained from the Protein Data Bank (PDB ID: 1TGU). To seek the binding sites of each OH-PAH in CAT, molecular docking was carried out as described in previous work (Chen et al., 2018). Afterwards, the conformation with the lowest binding free energy from docking results was chosen for further analysis. Besides, the Protein–Ligand Interaction Profiler (projects.biotec.tu-dresden.de/plip-web), a web service for fully automated detection of relevant non-covalent protein–ligand contacts in 3-D structures (Salentin, Schreiber, Haupt, Adasme, & Schroeder, 2015), was used to detect the interactions between each OH-PAH and its surrounding amino acid residues of the CAT molecule. Finally, PyMOL

software (the PyMOL Molecular Graphics System, Version 1.3r1 Schrödinger, LLC., NY, USA) was used to visualize and analyze the docking results (DeLano, 2002).

#### 2.2.4. CAT activity measurements

Catalase activity was determined using the method described in previous work (Chen et al., 2018). The activity measurements were performed at 17 °C. Each sample was tested for 6 times, and mean ± standard deviation was regarded as the final result. Statistical differences among various groups were analyzed using one-way analysis of variance (ANOVA) followed by Student's *t*-test (Chen et al., 2017). All data analyses were performed using SPSS 16.0 statistical software program for Windows (SPSS, Inc., Chicago, IL, USA). Values were considered statistically significant when $P < 0.05$.

## 3. Results and discussion

### 3.1. Effects of 1-OHNap, 9-OHPhe or 1-OHPyr on the fluorescence spectra of CAT

The intrinsic fluorescence of CAT is mainly attributed to its tryptophan (Trp) and tyrosine (Tyr) residues, and there are 6 Trp and 20 Tyr residues in each subunit of CAT (Schroeder et al., 1982). The fluorescence spectra of CAT with various concentrations of 1-OHNap, 9-OHPhe or 1-OHPyr were shown in Fig. 1. As shown in Fig. 1, pure CAT displays a strong fluorescence emission peak at 350 nm upon excitation at 280 nm. However, the fluorescence emission intensity of 1-OHNap, 9-OHPhe and 1-OHPyr can be ignored around 350 nm with identical excitation as shown in Fig. S1. The fluorescence intensity of CAT at the emission wavelength of 350 nm was obviously quenched with the addition of 1-OHNap, 9-OHPhe or 1-OHPyr, which indicated that an interaction had occurred between CAT and each OH-PAH. Moreover, isosbestic points were observed at 398 nm for 1-OHNap, 361 nm for 9-OHPhe and 376 nm for 1-OHPyr. This suggested the existence of the interaction equilibrium of each OH-PAHs-CAT system (Ghosh, Mitra, Pal, Basu, & Saha, 2017; Song et al., 2000). Interestingly, comparing the spectra of Fig. 1 and Fig. S1, there are inversions in the fluorescence intensity of 1-OHNap and 9-OHPhe in their maximum concentration in the presence and absence of CAT. It was because that CAT increased the fluorescence intensity of 1-OHNap, while decreased the intensity of 9-OHPhe. The relevant mechanism may be related to the varied interaction mechanism between the two compounds with CAT, which needs further investigation.

### 3.2. Fluorescence quenching mechanisms of CAT by 1-OHNap, 9-OHPhe or 1-OHPyr

The mechanisms of fluorescence quenching are usually classified as either dynamics quenching (collisional encounters) or static quenching (complex formation) (Zhang et al., 2016). In order to reveal the interaction mechanism of CAT with 1-OHNap, 9-OHPhe or 1-OHPyr, the fluorescence quenching spectra of CAT in the presence of different concentrations of individual OH-PAHs were measured under three different temperatures (17, 27 and 35 °C), and the fluorescence quenching data were analyzed according to the Stern–Volmer equation (Eq. S1) (Liu et al., 2017).

The Stern–Volmer plots for the quenching of CAT by OH-PAHs at three different temperatures were shown in Fig. S2. The values of the Stern–Volmer quenching constant ($K_{sv}$) and the quenching rate constant ($K_q$) were calculated and shown in Table S1. As can be seen from Fig. S2 and Table S1, the $K_{SV}$ values of 9-OHPhe-CAT and 1-OHPyr-CAT decreased with the increment of the temperature. Moreover, the $K_q$ values

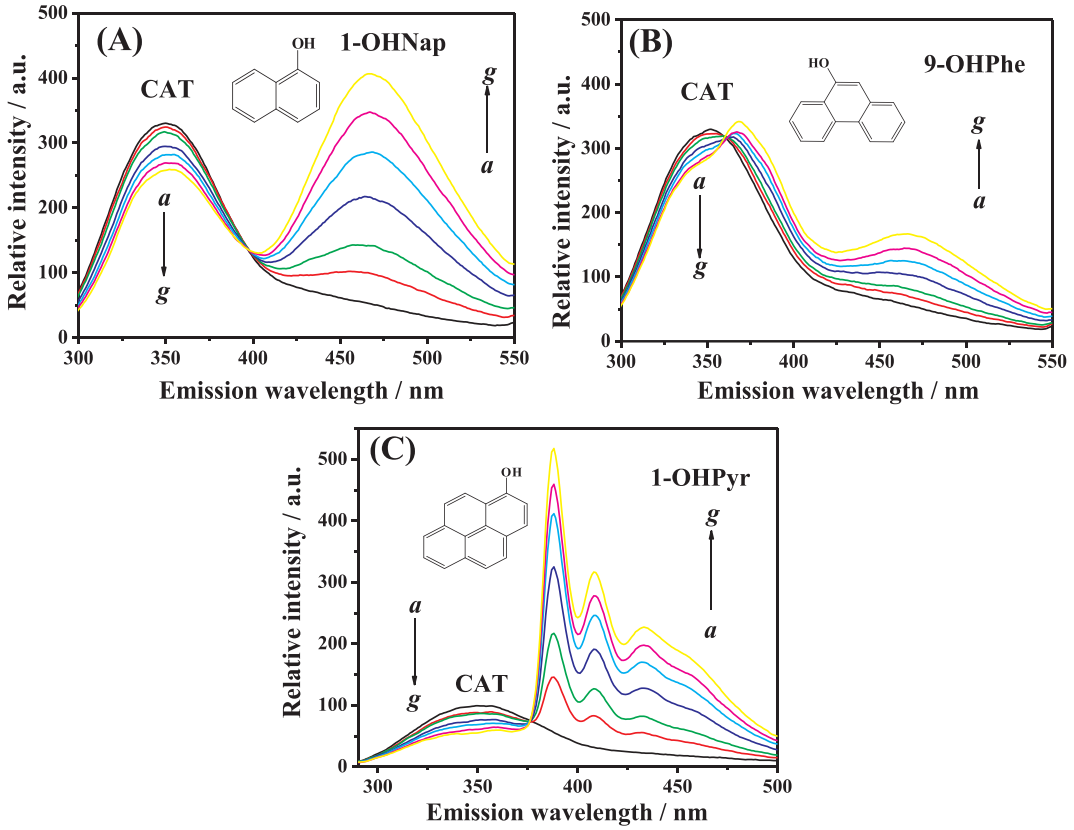


**Fig. 1.** Fluorescence quenching spectra of CAT in the presence of various concentrations of 1-OHNap (A), 9-OHPhe (B) and 1-OHPyr (Chen et al., 2015) (C) at 17 °C (pH = 7.40). Ex./Em. slit = 5/10 nm (A and B); Ex./Em. slit = 5/5 nm (C). c(CAT) = $1.0 \times 10^{-6}$ mol $L^{-1}$; c(CAT) = $1.0 \times 10^{-6}$ mol $L^{-1}$; c(1-OHNap), a-g: (0, 0.5, 1.0, 2.0, 3.0, 4.0, 5.0) × $10^{-5}$ mol $L^{-1}$; c(9-OHPhe), a-g: (0, 1.0, 2.0, 4.0, 6.0, 8.0, 10.0) × $10^{-6}$ mol $L^{-1}$; c(1-OHPyr), a-g: (0, 1.0, 2.0, 4.0, 6.0, 8.0, 10.0) × $10^{-6}$ mol $L^{-1}$.

of 9-OHPhe-CAT and 1-OHPyr-CAT were both much larger than the maximum dynamic quenching constant of the various quenchers ($2.0 \times 10^{10}$ L mol$^{-1}$ s$^{-1}$ (Liu et al., 2017)). These results indicated that the fluorescence quenching of CAT induced by 9-OHPhe or 1-OHPyr was a static process. While for 1-OHNap, the $K_{SV}$ values of 1-OHNap-CAT increased with the increment of the temperature, which indicated a dynamic process was involved. What's more, the $K_q$ values of 1-OHNap-CAT at three temperatures were higher than $2.0 \times 10^{10}$ L mol$^{-1}$ s$^{-1}$, indicating a static process also occurred. That is to say, a combined quenching process (both dynamic and static quenching) existed in the system of CAT and 1-OHNap (Zhang et al., 2016).

### 3.3. Binding parameters of 1-OHNap, 9-OHPhe, and 1-OHPyr with CAT

In order to get a better understanding of the static quenching process of CAT induced by the three OH-PAHs, investigation on the binding parameters (e.g., binding constant, number of binding sites, thermodynamic parameters, and binding distance) between CAT and OH-PAHs is necessary. Thus, a further research focused on the OH-PAHs-CAT binding interactions was performed.

#### 3.3.1. Binding constant ($K_b$) and the number of binding sites ($n$) of each OH-PAH with CAT

When OH-PAHs molecules are bound independently to a set of equivalent sites on CAT macromolecule, the $K_b$ and $n$ values can be obtained by the double logarithm equation (Eq. S2) (Jahanban-Esfahlan & Panahi-Azar, 2016). The values of $K_b$ and $n$ at three different temperatures were shown in Table 1. As can be seen in Table 1, the $K_b$ values of the 1-OHNap–CAT, 9-OHPhe–CAT and 1-OHPyr–CAT complexes were $6.31 \times 10^3$, $1.03 \times 10^4$ and $2.96 \times 10^5$ L mol$^{-1}$ at 17 °C, indicating that the binding capacity of the three OH-PAHs with CAT increased with the increment of the number of benzene rings under this experimental condition. Moreover, the $n$ values were all approximately equal to 1 for the three OH-PAHs-CAT systems at 17 °C, which indicated that there was one binding site for each OH-PAH in CAT at this temperature. The values of $K_b$ and $n$ of the three systems all decreased at higher temperatures, which demonstrated that higher temperature hindered the formation of the OH-PAH-CAT complex.

Moreover, the binding constants of the three OH-PAHs with CAT were in the order of 1-OHNap < 9-OHPhe < 1-OHPyr at 17 and 27 °C. Meanwhile, the octanol/water partition coefficients (log$K_{ow}$) of 1-OHNap, 9-OHPhe and 1-OHPyr are 2.689, 3.865 and 4.453, which is in the same order as the binding constants at the two temperatures. This suggested that the hydrophobicity of OH-PAHs could affect their affinities to CAT, which was also revealed by previous study that focused on the binding of organic ligands with protein (Zhang et al., 2013). While at 35 °C, the order of the binding constants turned into 9-OHPhe < 1-OHNap < 1-OHPyr. This interesting phenomenon can be well explained by the thermodynamic parameters presented in Section 3.3.2. As $\Delta H < 0$, the binding interactions of the three OH-PAHs with CAT were exothermic. Thus, the binding affinity of OH-PAHs with CAT decreased with the increment of temperature for each system. As $|\Delta H|$ of 9-OHPhe with CAT was larger than that of 1-OHNap, the binding of 9-OHPhe with CAT was more susceptible to temperature than 1-OHNap. Therefore, the binding affinity of 9-OHPhe with CAT decreased to a value which was lower than that of 1-OHNap at 35 °C, which was different from the order at 17 and 27 °C.

**Table 1**
Binding constants ($K_b$) and binding sites ($n$) of the 1-OHNap-CAT, 9-OHPhe-CAT and 1-OHPyr-CAT interactions.

| | $T$/°C | $K_b$/L mol$^{-1}$ | $n$ | $R^2$ |
|---|---|---|---|---|
| 1-OHNap-CAT | 17 | $6.31 \times 10^3$ | 1.08 | 0.996 |
| | 27 | $7.12 \times 10^2$ | 0.790 | 0.979 |
| | 35 | $5.09 \times 10^2$ | 0.733 | 0.991 |
| 9-OHPhe-CAT | 17 | $1.03 \times 10^4$ | 0.948 | 0.997 |
| | 27 | $1.63 \times 10^3$ | 0.782 | 0.978 |
| | 35 | $3.49 \times 10^2$ | 0.654 | 0.985 |
| 1-OHPyr-CAT | 17 | $2.96 \times 10^5$ | 1.11 | 0.995 |
| (Chen et al., 2015) | 27 | $1.62 \times 10^5$ | 1.07 | 0.994 |
| | 35 | $5.54 \times 10^4$ | 0.982 | 0.995 |

#### 3.3.2. Thermodynamic parameters in the binding of the OH-PAHs with CAT

The binding forces between biomolecules and small molecular ligands mainly include hydrophobic interactions, hydrogen bonds, van der Waals interactions, and electrostatic forces. The type of binding forces dominated in the binding process can be determined based on enthalpic change ($\Delta H$) and entropic change ($\Delta S$) of the interactions (Ross & Subramanian, 1981). Because the temperature range was not too wide (from 17 °C to 35 °C), the $\Delta H$ could be regarded as a constant. Therefore, the thermodynamic parameters $\Delta H$, $\Delta S$, and $\Delta G$ (the free energy change) could be calculated using the Van't Hoff equation (Fq. S3) and thermodynamic equation (Fq. S4). The $\Delta H$ and $\Delta S$ values were calculated from the slope and intercept values of the plot of ln$K_b$ *versus* 1/T, respectively. The calculated thermodynamic parameters of the binding of CAT with each OH-PAH were listed in Table S2. As can be seen, $\Delta G < 0$ revealed that the binding interactions were all spontaneous; $\Delta H < 0$ indicated that the binding interaction in each system was an exothermic process. As $\Delta G < 0$, $\Delta H < 0$ and $-T\Delta S > 0$, it suggested that the binding process was enthalpy-driven (Pan, Jiang, Liu, Wang, & Shi, 2017). All in all, the binding interactions between the three OH-PAHs and CAT were spontaneous, exothermic and enthalpy-driven. Moreover, the negative $\Delta H$ and negative $\Delta S$ indicated that van der Waals and hydrogen bonds forces played major roles in the binding process of all the three OH-PAHs with CAT (Mu et al., 2019).

#### 3.3.3. Binding distances of the OH-PAHs with CAT

Fluorescence resonance energy transfer (FRET) is a useful technique to determine the distance between a donor (fluorophore) and an acceptor. As the absorption spectrum of each OH-PAH and the fluorescence emission spectrum of CAT overlap enough (Fig. S3), the energy transfer from CAT to OH-PAHs may happen with a high probability (Förster, 1965). Herein, the average distances between the TRP residues of CAT and each OH-PAH were investigated using FRET. After fitting data to Eqs. (S5) – (S7), all of the calculated parameters were shown in Table S3.

As shown in Table S3, the energy transfer efficiency ($E$) of CAT to 1-OHNap, 9-OHPhe and 1-OHPyr was 3.83%, 4.05% and 11.83%, respectively. The average distances from the TRP residue of CAT to 1-OHNap, 9-OHPhe and 1-OHPyr ($r$) were 3.28, 4.06 and 3.48 nm, which were all less than 7 nm. This confirmed that there is a high probability of energy transfer from CAT to each OH-PAH. Moreover, it demonstrated again that the static quenching process occurred in the interactions between OH-PAHs and CAT.

### 3.4. Molecular docking of the OH-PAHs with CAT

To further locate the specific binding site of each OH-PAH in CAT and obtain more detailed binding information at the molecular level, blind molecular docking method was utilized to reveal the optimal binding mode of each OH-PAH with CAT. During the docking simulations, the lowest energy-ranked binding mode was chosen among 25 conformers of docking results in each OH-PAH-CAT system. The obtained optimal locations of each OH-PAH on CAT and the specific interactions between OH-PAHs and its surrounding amino acid residues were shown in Fig. 2. The relevant information was listed in Tables S4–S7.

As illustrated in Fig. 2A, C and E, the three OH-PAHs were all located near the active center (Heme) of CAT, which indicated that the three OH-PAHs might make impact on the activity of CAT. Fig. 2B, D

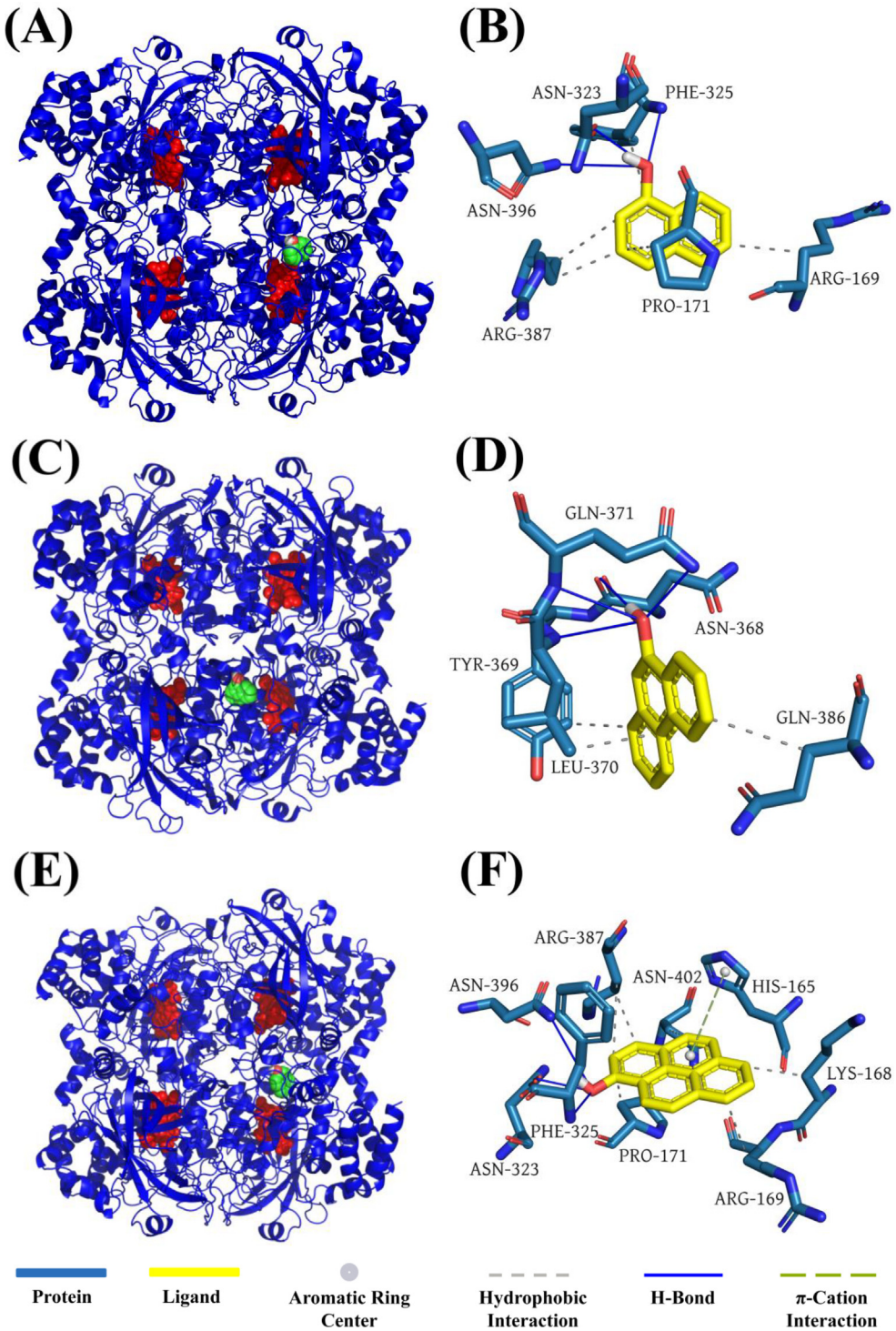


**Fig. 2.** The binding modes of three OH-PAHs to CAT. Binding site of 1-OHNap (A), 9-OHPhe (C), and 1-OHPyr (E) in CAT; Detailed illustration of the binding forces of 1-OHNap (B), 9-OHPhe (D), and 1-OHPyr (F) with the surrounding amino acid residues.

and F illustrates the neighboring amino acid residues around each OH-PAH, and also the varied non-covalent interactions between these amino acid residues and each OH-PAH. As can be seen in Fig. 2B and Table S4, 1-OHNap formed hydrophobic interactions with ARG169, PRO171, PHE325 and ARG387; three hydrogen bonds were formed between 1-OHNap and ASN323, PHE325, ASN396, with the bond length of 1.87 Å, 1.74 Å, and 3.68 Å, respectively. 9-OHPhe had hydrophobic contacts with TYR369, LEU370, and GLN386; there were four hydrogen bonds formed between 9-OHPhe and CAT, one between 9-OHPhe and ASN368 (2.10 Å), one between 9-OHPhe and LEU370 (3.05 Å), and two between 9-OHPhe and GLN 371 (3.11 Å and 2.45 Å) (Fig. 2D and Table S5). As for 1-OHPyr (Fig. 2F and Table S6), hydrophobic interactions were formed between 1-OHPyr and LYS168, ARG169, PRO171, ARG387, ASN402; three hydrogen bonds were observed between 1-OHPyr and ASN323, PHE325, ASN396, with the bond length of 1.82 Å, 1.98 Å, and 3.58 Å, respectively; moreover, a benzene ring of 1-OHPyr and the heterocyclic ring of HIS165 were closely packed in parallel and had the π-Stacking interactions which could enhance the binding of 1-OHPyr to CAT. Combined the results in thermomechanical analysis and theoretical studies, it suggested that

van der Waals interactions, hydrogen bonds and hydrophobic interactions played major roles in the binding of three OH-PAHs with CAT.

Moreover, for the selected conformations, the $K_b$ values calculated from the docking studies of the OH-PAHs-CAT systems were ranked in 1-OHNap < 9-OHPhe < 1-OHPyr (as shown in Table S7). The results were consistent with the experimental results by fluorescence analysis, indicating that molecular docking technique was reliable to study the binding interactions between CAT and OH-PAHs. In addition, for the three OH-PAHs-CAT systems, the discrepancies between the estimated $K_b$ values and experimental $K_b$ values may be due to the fact that the X-ray structure of the CAT crystals used in the molecular docking study was different from that of the aqueous system reported previously (Sharma, Anandakumar, & Ilanchelian, 2014).

### 3.5. Effects of the OH-PAHs on the conformation of CAT

It had been confirmed that the interactions of each OH-PAHs with CAT could cause the fluorescence characteristics change of the CAT. However, it was still unclear whether the binding interactions could influence the microenvironment and conformation of the CAT, and whether the effects varied among the three OH-PAHs. In order to address these issues, the synchronous fluorescence and CD spectroscopy were employed to investigate the structural changes of the CAT when binding with OH-PAHs in the following sections.

#### 3.5.1. Effects of OH-PAHs on the synchronous fluorescence spectra of CAT

Synchronous fluorescence spectroscopy can be used to characterize the microenvironmental changes around chromosphere molecules like Tyr or Trp residues in CAT (Chen et al., 2018). The synchronous fluorescence spectra of CAT in the presence of different concentrations of OH-PAHs were shown in Fig. 3. With the addition of each OH-PAH, the synchronous fluorescence intensity of Trp ($\Delta\lambda = 60$ nm) and Tyr ($\Delta\lambda = 15$ nm) residues both decreased. Meanwhile, the maximum emission wavelength of Trp and Tyr residues had no obvious shift with the addition of 1-OHNap and 9-OHPhe. It indicated that neither 1-OHNap nor 9-OHPhe did perturb the polarity of microenvironment around Trp and Tyr residues significantly. However, the maximum emission wavelength of Trp residues had a distinct red shift (from 282 to 286 nm) with the addition of 1-OHPyr (Fig. 3C), which indicated that the Trp residues were placed in a less hydrophobic environment (Xu et al., 2018). Moreover, the $K_{sv}$ values for Tyr and Trp residues in each OH-PAHs-CAT system were calculated and shown in Table S8. The results suggested that 1-OHNap and 9-OHPhe induced greater perturbation of the microenvironment around Tyr than Trp residues, while 1-OHPyr showed a greater effect on Trp than Tyr residues.

#### 3.5.2. Effects of the OH-PAHs on the circular dichroism (CD) spectra of CAT

In order to quantitatively study the effects of the OH-PAHs on the secondary structure of CAT, CD spectroscopy was further performed in the absence and presence of the OH-PAHs. As shown in Fig. S4, the CD spectra of pure CAT exhibits two main negative bands at approximately 210 and 220 nm, which characters the α-helix structure of CAT (Wang et al., 2016). With the addition of 1-OHNap and 1-OHPyr, the intensity of the two negative bands of CAT increased, while the intensity of the two bands decreased in 9-OHPhe-CAT system, inferring considerable changes in the secondary structure of CAT induced by OH-PAHs.

Furthermore, the CD data were quantitatively analyzed using the CDPro software package, and the results of the secondary structural contents of CAT in each system were listed in Table 2. As shown in Table 2, compared with pure CAT, the secondary structural contents of CAT altered differently after the addition of OH-PAHs. With a molar ratio of 1-OHNap or 1-OHPyr to CAT at 20:1, there is approximately a 1.7% and 2.7% increase of α-helix, respectively, with a corresponding decrease of β-sheet. It suggested that 1-OHNap and 1-OHPyr could stabilize the conformation of CAT to a certain extent, mainly by increasing the helix content. While, the α-helix content decreased approximately 2.4% with a molar ratio of 9-OHPhe to CAT at 20:1, with an accompanying increase of β-sheet. It was probably because 9-OHPhe interacts with certain amino acid residues in CAT, thus destroyed the hydrogen bonding networks of the CAT, inducing the transformation of helical structure of the CAT to sheets (Xu et al., 2018). Therefore, the three OH-PAHs induced varied structure changes of CAT, which mainly due to their different molecular interactions with CAT.

### 3.6. Effects of the OH-PAHs on the activity of CAT

The biological activity of CAT can be used as a sensitive biomarker of contaminant-induced oxidative stress in organisms (Glorieux & Calderon, 2017). As the structural changes of CAT induced by OH-PAHs may alter the activity of CAT, the activity determination is needed for exploring the adverse effect of each OH-PAH on CAT. The effects of different concentrations of OH-PAHs ranging from 0 to $1.0 \times 10^{-5}$ mol L$^{-1}$ or $5.0 \times 10^{-5}$ mol L$^{-1}$ on CAT activity ($1.0 \times 10^{-6}$ mol L$^{-1}$) were tested *in vitro* and the results are presented in Fig. 4 and Table S9. As can be seen from Fig. 4, the activity of CAT had no obvious change at lower concentrations of 1-OHNap (from 0 to $2.0 \times 10^{-5}$ mol L$^{-1}$); while CAT activity trended to decrease with further increase of 1-OHNap concentration, and decreased to 91.6% of the initial level at the highest experimental concentration of 1-OHNap ($5.0 \times 10^{-5}$ mol L$^{-1}$). The activity of CAT increased gradually to 105.0% of its initial level at the concentration ratio of 9-OHPhe to CAT below 6:1, and slightly decreased with the continuous increment of 9-OHPhe (from $6.0 \times 10^{-6}$ to $1.0 \times 10^{-5}$ mol L$^{-1}$). While, the relative activity of CAT remained unchangeable when 1-OHPyr concentration was lower than $2.0 \times 10^{-6}$ mol L$^{-1}$, and obviously decreased with further increase of 1-OHPyr concentration (to 86.8% of its initial level at 1-OHPyr/CAT = 10:1). Combined with the CD spectral results, the promotion effects of 9-OHPhe on CAT activity may be attributed to the decrease of the helix of CAT and the loosening of CAT structure, which make the substrate channel of CAT easier to get through for $H_2O_2$ and increase the chance for $H_2O_2$ to contact with heme (Moradi, Divsalar, Saboury, Ghalandari, & Harifi, 2015; Rashtbari, Dehghan, Yekta, Jouyban, & Iranshahi, 2017; Rui, Liu, & Zong, 2016). While, the CAT activity slightly decreased at higher concentrations of 9-OHPhe, which was probably because that the structure of the active center of CAT was destroyed by the excess 9-OHPhe (Chen et al., 2018). In addition, 1-OHNap and 1-OHPyr induced the increase of the helix of CAT and thus make the structure of CAT even tighter, which might hinder the contact of $H_2O_2$ with heme, and resulted in the inhibition of CAT activity.

It can be seen from Table S9, compared the effects of the three OH-PAHs on CAT activity at the identical concentration level ($1.0 \times 10^{-5}$ mol L$^{-1}$), their influence degree on CAT activity was in the order of 1-OHNap < 9-OHPhe < 1-OHPyr. This indicated that the effects of the three OH-PAHs on the activity of CAT were associated with the binding affinity of OH-PAHs to CAT, which increased with the increment of the number of benzene rings of OH-PAHs. As the activity inhibition of CAT can cause the enhanced generation of ROS (Lee et al., 2018; Najjar et al., 2016), 1-OHNap and 1-OHPyr are more likely to induce oxidative stress than 9-OHPhe *in vivo*. Some research had pointed out that PAHs could undergo oxidative metabolism *in vivo* and produced a large amount of reactive oxygen species, hence the induced oxidative stress will change the activity of CAT (Ranjit et al., 2016; Singh, Patel, Jyoti, Ram, Mathur, & Siddiqui, 2008). Herein, the above results further suggested that the oxidative metabolites of PAHs might also cause direct adverse effects on CAT in organism.

## 4. Conclusion

In this study, the interactions of three OH-PAHs with CAT and the corresponding effects on the structure and function of CAT at the molecular level were investigated using experimental studies and

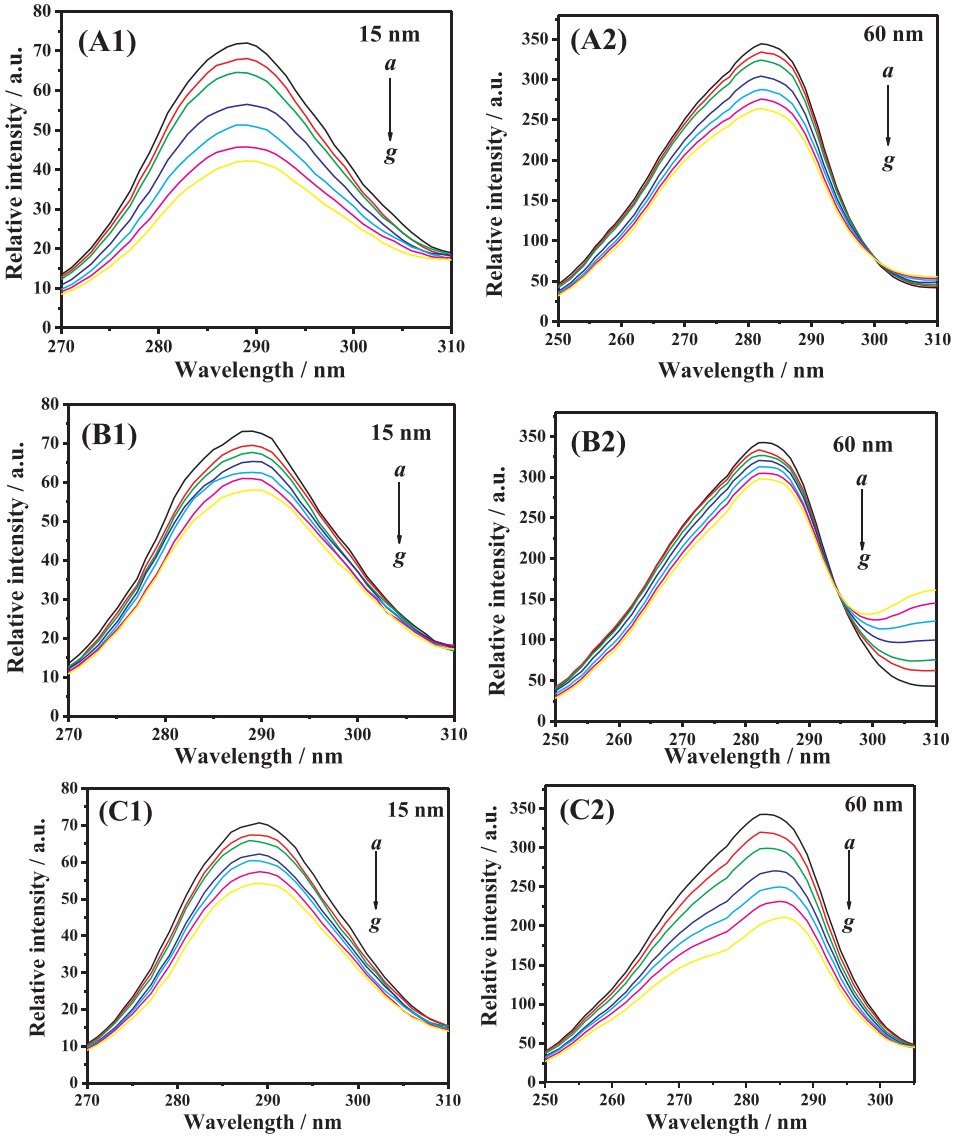


**Fig. 3.** Synchronous fluorescence spectra of the 1-OHNap-CAT (A), 9-OHPhe-CAT (B) and 1-OHPyr-CAT (Chen et al., 2015) (C) systems at 17 °C (pH = 7.40). *c* (CAT) = $1.0 \times 10^{-6}$ mol $L^{-1}$; *c*(1-OHNap), a-g: (0, 0.5, 1.0, 2.0, 3.0, 4.0, 5.0) × $10^{-5}$ mol $L^{-1}$; *c*(9-OHPhe), a-g: (0, 1.0, 2.0, 4.0, 6.0, 8.0, 10.0) × $10^{-6}$ mol $L^{-1}$; *c* (1-OHPyr), a-g: (0, 1.0, 2.0, 4.0, 6.0, 8.0, 10.0) × $10^{-6}$ mol $L^{-1}$.

**Table 2**
Secondary structure contents of CAT in presence of different molar ratios of OH-PAHs.

| OH-PAHs | *c*(OH-PAHs)/*c* (CAT) | Secondary structural elements in CAT | | | |
|---|---|---|---|---|---|
| | | α-helix/% | β-sheet/% | β-turn/% | Random coil/ % |
| 1-OHNap | 0:1 | 20.1 | 27.3 | 21.1 | 31.5 |
| | 1:1 | 20.9 | 27.0 | 20.9 | 31.3 |
| | 20:1 | 21.8 | 26.4 | 20.6 | 31.2 |
| 9-OHPhe | 1:1 | 19.8 | 27.8 | 20.7 | 31.7 |
| | 20:1 | 17.7 | 29.1 | 20.9 | 32.3 |
| 1-OHPyr | 1:1 | 21.2 | 25.6 | 21.8 | 31.4 |
| | 20:1 | 22.8 | 24.2 | 22.7 | 30.3 |

molecular docking. The results showed that 1) the binding affinity of the three OH-PAHs with CAT increased with the increment of the number of benzene rings at 17 and 27 °C, as the hydrophobicity of OH-PAHs could affect their binding ability to CAT. However, the order of the binding constants at 35 °C was different from that at 17 and 27 °C, as the increase of temperature inhibited the binding affinities of the three OH-PAHs with CAT to varied extent. Van der Waals' force, hydrogen bonds and hydrophobic interactions played important roles in the binding interactions of CAT with the three OH-PAHs. The binding distances of 1-OHNap, 9-OHPhe, and 1-OHPyr with CAT were determined to be 3.28, 4.06 and 3.48 nm. 2) OH-PAHs with different numbers of aromatic rings can induce different structural changes of CAT. Specifically, 1-OHNap and 9-OHPhe induced greater perturbation of the microenvironment around Tyr residues, while 1-OHPyr showed a greater effect on Trp residues. Both 1-OHNap and 1-OHPyr affected the secondary structure of CAT by increasing the content of α-helix, while 9-OHPhe destroyed the helix of CAT. 3) The activity of CAT can be inhibited by both 1-OHNap and 1-OHPyr at experimental concentrations. While, 9-OHPhe has a continuous promotion effects on CAT activity at lower concentrations ($< 6.0 \times 10^{-6}$ mol $L^{-1}$), but the promotion slightly decreased at higher concentrations. At the concentration of $1.0 \times 10^{-5}$ mol $L^{-1}$, the effect degree of 1-OHNap, 9-OHPhe and 1-OHPyr on CAT activity was in the order of 1-OHNap < 9-OHPhe < 1-OHPyr. Overall, the results demonstrated that the varied effects of the three OH-PAHs on CAT were closely

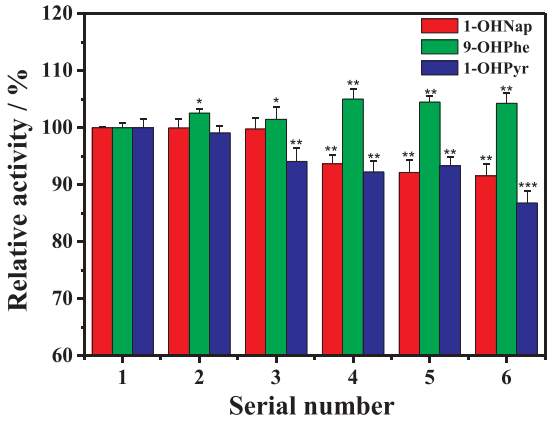


**Fig. 4.** Effects of different concentrations of 1-OHNap, 9-OHPhe and 1-OHPyr on the activity of CAT at 17 °C (pH = 7.40). $c$(CAT) = $1.0 \times 10^{-6}$ mol $L^{-1}$; $c$(1-OHNap), 1–6: (0, 1.0, 2.0, 3.0, 4.0, 5.0) × $10^{-5}$ mol $L^{-1}$; $c$(9-OHPhe), 1–6: (0, 2.0, 4.0, 6.0, 8.0, 10.0) × $10^{-6}$ mol $L^{-1}$; $c$(1-OHPyr), 1–6: (0, 2.0, 4.0, 6.0, 8.0, 10.0) × $10^{-6}$ mol $L^{-1}$. (n = 6. *, $P < 0.05$ vs. control; **, $P < 0.01$ vs. control; ***, $P < 0.001$ vs. control).

related to the different molecular interactions of the three OH-PAHs with CAT. The *in-vitro* adverse effects of OH-PAHs on CAT indicated that OH-PAHs may cause the oxidative stress *in vivo*, and warned the health risk of the PAHs through food intake.

Overview, this work provided useful data for clarifying the molecular interaction mechanism of OH-PAHs with CAT. While, considering the limitations of this work, further investigations need to be conducted on the issues which were not yet figured out in the present study. For instance, the specific proportion of static and dynamic quenching in combined quenching mechanism of 1-OHNap on CAT, the in-depth reason for the inversions in fluorescence intensity of 1-OHNap and 9-OHPhe with and without CAT, and the structural changes of CAT around its Trp or Tyr residues induced by OH-PAHs and the corresponding effects on Trp or Tyr. Meanwhile, some other techniques such as ITC, NMR and molecular dynamics simulations can be applied to further study the molecular interactions between OH-PAHs and CAT. Moreover, more research efforts are expected to investigate the molecular interactions of OH-PAHs with other antioxidant enzymes as GPX, SOD and GST.

## Declaration of Competing Interest

The authors declare that they have no known competing financial interests or personal relationships that could have appeared to influence the work reported in this paper.

## Acknowledgments

We gratefully acknowledge the financial support of the National Major Scientific Instruments Development Project of China [grant number 21627814], the National Natural Science Foundation of China [grant number 21577110], the Natural Science Foundation of Fujian Province [grant number 2018J05024] and the Program for Prominent Young Talents in Fujian Province University, China [grant number [2018]47].

## Appendix A. Supplementary data

Supplementary data to this article can be found online at https://doi.org/10.1016/j.foodchem.2019.125743.

## References

Chen, L., Zhang, J., Zhu, Y., & Zhang, Y. (2015). Molecular interactions of 1-hydroxypyrene with catalase revealed by spectroscopic methods combined with molecular docking. *Chemical Journal of Chinese Universities-Chinese, 36*(12), 2394–2401.
Chen, L., Zhang, J., Zhu, Y., & Zhang, Y. (2018). Interaction of chromium (III) or chromium (VI) with catalase and its effect on the structure and function of catalase: An in vitro study. *Food Chemistry, 244*, 378–385.
Chen, X. P., Dong, Q. X., Chen, Y. H., Zhang, Z. X., Huang, C. J., Zhu, Y. X., & Zhang, Y. (2017). Effects of Dechlorane Plus exposure on axonal growth, musculature and motor behavior in embryo-larval zebrafish. *Environmental Pollution, 224*, 7–15.
Deisseroth, A., & Dounce, A. L. (1970). Catalase: Physical and chemical properties, mechanism of catalysis, and physiological role. *Physiological Reviews, 50*(3), 319–375.
DeLano, W. L. (2002). The PyMOL molecular graphics system.
Diamante, G., Muller, G., Menjivar-Cervantes, N., Xu, E. G., Volz, D. C., Bainy, A. C. D., & Schlenk, D. (2017). Developmental toxicity of hydroxylated chrysene metabolites in zebrafish embryos. *Aquatic Toxicology, 189*, 77–86.
Förster, T. (1965). *Delocalized excitation and excitation transfer*. Florida State University, Tallahassee: Florida State University.
Frisch, M., Trucks, G., Schlegel, H. B., Scuseria, G., Robb, M., Cheeseman, J., Scalmani, G., Barone, V., Mennucci, B., & Petersson, G. (2009). Gaussian 09, Revision A. 02, Gaussian. Inc., Wallingford, CT, 200.
Ghosh, S., Mitra, A. K., Pal, U., Basu, S., & Saha, C. (2017). Evidence of two structurally related solvatochromic probes complexed with beta-cyclodextrin by using spectroscopic methods. *Journal of Molecular Structure, 1130*, 810–817.
Glorieux, C., & Calderon, P. B. (2017). Catalase, a remarkable enzyme: Targeting the oldest antioxidant enzyme to find a new cancer treatment approach. *Biological Chemistry, 398*(10), 1095–1108.
Gysel, N., Dixit, P., Schmitz, D. A., Engling, G., Cho, A. K., Cocker, D. R., & Karavalakis, G. (2018). Chemical speciation, including polycyclic aromatic hydrocarbons (PAHs), and toxicity of particles emitted from meat cooking operations. *Science of the Total Environment, 633*, 1429–1436.
Jahanban-Esfahlan, A., & Panahi-Azar, V. (2016). Interaction of glutathione with bovine serum albumin: Spectroscopy and molecular docking. *Food chemistry, 202*, 426–431.
Lao, J. Y., Xie, S. Y., Wu, C. C., Bao, L. J., Tao, S., & Zeng, E. Y. (2018). Importance of dermal absorption of polycyclic aromatic hydrocarbons derived from barbecue fumes. *Environmental Science & Technology, 52*(15), 8330–8338.
Lee, J. N., Dutta, R. K., Maharjan, Y., Liu, Z. Q., Lim, J. Y., Kim, S. J., ... Park, R. (2018). Catalase inhibition induces pexophagy through ROS accumulation. *Biochemical and Biophysical Research Communications, 501*(3), 696–702.
Li, F., Li, X., Liu, X., Zhang, L., You, L., Zhao, J., & Wu, H. (2011). Noncovalent interactions between hydroxylated polycyclic aromatic hydrocarbon and DNA: Molecular docking and QSAR study. *Environmental Toxicology & Pharmacology, 32*(3), 373–381.
Liu, B., Xiao, H., Li, J., Geng, S., Ma, H., & Liang, G. (2017). Interaction of phenolic acids with trypsin: Experimental and molecular modeling studies. *Food chemistry, 228*, 1–6.
Moorthy, B., Chu, C., & Carlin, D. J. (2015). Polycyclic aromatic hydrocarbons: From metabolism to lung cancer. *Toxicological Sciences, 145*(1), 5–15.
Moradi, M., Divsalar, A., Saboury, A. A., Ghalandari, B., & Harifi, A. R. (2015). Inhibitory effects of deferasirox on the structure and function of bovine liver catalase: A spectroscopic and theoretical study. *Journal of Biomolecular Structure & Dynamics, 33*(10), 2255–2266.
Morris, G. M., Huey, R., Lindstrom, W., Sanner, M. F., Belew, R. K., Goodsell, D. S., & Olson, A. J. (2009). AutoDock4 and AutoDockTools4: Automated docking with selective receptor flexibility. *Journal of Computational Chemistry, 30*(16), 2785–2791.
Mu, H., Chen, S., Liu, F., Xiao, J., Huang, H., Zhang, Y., ... Yuan, X. (2019). Stereoselective interactions of lactic acid enantiomers with HSA: Spectroscopy and docking application. *Food chemistry, 270*, 429–435.
Najjar, F. M., Ghadari, R., Yousefi, R., Safari, N., Sheikhhasani, V., Sheibani, N., & Moosavimovahedi, A. A. (2016). Studies to reveal the nature of interactions between catalase and curcumin using computational methods and optical techniques. *International journal of biological macromolecules, 95*, 550–556.
Ohura, T., Kurihara, R., & Hashimoto, S. (2010). Aryl hydrocarbon receptor activities of hydroxylated polycyclic aromatic hydrocarbons in recombinant yeast cells. *Toxicological & Environmental Chemistry Reviews, 92*(4), 737–742.
Pan, D. Q., Jiang, M., Liu, T. T., Wang, Q., & Shi, J. H. (2017). Combined spectroscopies and molecular docking approach to characterizing the binding interaction of enalapril with bovine serum albumin. *Luminescence, 32*(4), 481–490.
Ranjit, S., Midde, N. M., Sinha, N., Patters, B. J., Rahman, M. A., Cory, T. J., ... Kumar, S. (2016). Effect of polyaryl hydrocarbons on cytotoxicity in monocytic cells: Potential role of cytochromes P450 and oxidative stress pathways. *PloS one, 11*(9), e0163827.
Rashtbari, S., Dehghan, G., Yekta, R., Jouyban, A., & Iranshahi, M. (2017). Effects of resveratrol on the structure and catalytic function of bovine liver catalase (BLC): Spectroscopic and theoretical studies. *Advanced Pharmaceutical Bulletin, 7*(3), 349–357.
Ross, P. D., & Subramanian, S. (1981). Thermodynamics of protein association reactions: Forces contributing to stability. *Biochemistry, 20*(11), 3096–3102.
Rui, Z., Liu, R., & Zong, W. (2016). Bisphenol S interacts with catalase and induces oxidative stress in mouse liver and renal cells. *Journal of Agriculture and Food Chemistry, 64*(34), 6630–6640.
Salentin, S., Schreiber, S., Haupt, V. J., Adasme, M. F., & Schroeder, M. (2015). PLIP: Fully automated protein-ligand interaction profiler. *Nucleic Acids Research, 43*(W1), W443–W447.
Schroeder, W. A., Shelton, J. R., Shelton, J. B., Robberson, B., Apell, G., Fang, R. S., & Bonaventura, J. (1982). The complete amino acid sequence of bovine liver catalase and the partial sequence of bovine erythrocyte catalase. *Archives of Biochemistry and*

*Biophysics. 214*(1), 397–421.
Sharma, A. S., Anandakumar, S., & Ilanchelian, M. (2014). A combined spectroscopic and molecular docking study on site selective binding interaction of Toluidine blue O with human and bovine serum albumins. *Journal of Luminescence, 151*(10), 206–218.
Sievers, C. K., Shanle, E. K., Bradfield, C. A., & Xu, W. (2013). Differential action of monohydroxylated polycyclic aromatic hydrocarbons with estrogen receptors α and β. *Toxicological Sciences, 132*(2), 359–367.
Singh, V. K., Patel, D. K., Jyoti, Ram S., Mathur, N., & Siddiqui, M. K. J. (2008). Blood levels of polycyclic aromatic hydrocarbons in children and their association with oxidative stress indices: An Indian perspective. *Clinical Biochemistry, 41*(3), 152–161.
Song, Y. M., Kang, J. W., Zhou, J., Wang, Z. H., Lu, X. Q., Wang, L. F., & Gao, J. Z. (2000). Study on the fluorescence spectra and electrochemical behavior of $ZnL_2$ and Morin with DNA. *Spectrochimica Acta Part A: Molecular and Biomolecular Spectroscopy, 56*(12), 2491–2497.
Wang, J., Wang, J., Xu, C., Liu, R., & Chen, Y. (2016). Molecular mechanism of catalase activity change under sodium dodecyl sulfate-induced oxidative stress in the mouse primary hepatocytes. *Journal of Hazardous Materials, 307*, 173–183.
Wang, L. R., Wang, Y., Chen, J. W., & Guo, L. H. (2009). A structure-based investigation on the binding interaction of hydroxylated polycyclic aromatic hydrocarbons with DNA. *Toxicology, 262*(3), 250–257.
Wu, T., Wu, Q., Guan, S., Su, H., & Cai, Z. (2007). Binding of the environmental pollutant naphthol to bovine serum albumin. *Biomacromolecules, 8*(6), 1899–1906.
Xu, M., Cui, Z., Zhao, L., Hu, S., Zong, W., & Liu, R. (2018). Characterizing the binding interactions of PFOA and PFOS with catalase at the molecular level. *Chemosphere, 203*, 360–367.
Zhang, F., Zhang, J., Tong, C. L., Chen, Y. D., Zhuang, S. L., & Liu, W. P. (2013). Molecular interactions of benzophenone UV filters with human serum albumin revealed by spectroscopic techniques and molecular modeling. *Journal of Hazardous Materials, 263*, 618–626.
Zhang, J., Chen, W., Tang, B., Zhang, W., Chen, L., Duan, Y., ... Zhang, Y. (2016). Interactions of 1-hydroxypyrene with bovine serum albumin: Insights from multi-spectroscopy, docking and molecular dynamics simulation methods. *RSC Advances, 6*(28), 23622–23633.